Bayesian inference approach for Full Poincaré Mueller polarimetry

Juan Carlos Suárez-Bermejo[1], Javier Gorgas[1,1], Sergio Pascual[1,1], Massimo Santarsiero[1], Juan Carlos González de Sande[1], Gemma Piquero[1]

Abstract

Full Poincaré Mueller Polarimetry is a new technique for characterizing samples by means of their Mueller matrix. The method is based on the use of a full Poincaré beam as a generator of polarization states. These beams present different polarization states, covering the entire Poincaré sphere surface, at different points in the beam cross section. To obtain the Mueller matrix, Stokes parameters are collected at both the entrance and the output of the sample. They are calculated from irradiance measurements at each pixel of a CCD camera for different configurations of the polarization state analyzer. These measurements can be processed in several ways. In this work, we propose to use Bayesian inference, in particular, Markov chain Monte Carlo methods, to obtain, without any *prior* knowledge of the sample, its Mueller matrix together with its uncertainties. The new approach is tested with experimental measurements of different samples and compared with the real theoretical Mueller matrices. Excellent agreement is observed between the experimental results and the theoretical ones for all the samples tested.

Keywords: Polarimetry, Polarization, Full Poincaré beams, Bayesian inference

Email addresses: juancarlos.suarez@upm.es (Juan Carlos Suárez-Bermejo), jgorgas@fis.ucm.es (Javier Gorgas), sergiopr@fis.ucm.es (Sergio Pascual), massimo.santarsiero@uniroma3.it (Massimo Santarsiero), juancarlos.gonzalez@upm.es (Juan Carlos González de Sande), piquero@ucm.es (Gemma Piquero)

1. Introduction

Mueller matrix polarimetry is a noninvasive technique to obtain the linear optical properties of a sample, properties that are related to different characteristics such as composition, structure, thickness, surface roughness, etc. [1–4]. Determining these characteristics is essential in the manufacture and quality control of technological materials [2, 5–9], in medical diagnostic techniques [4, 10–15], in the measurement of air and water pollution [16–19], etc.

Numerous procedures have been developed to measure the Mueller matrix of a sample [1–3, 12, 20–26]. As a general rule, to determine the Mueller matrix of a sample it is necessary to use incident light with different polarization states and analyze the polarization state of the light at the output [1–3]. Modulation of the polarization state of light can be achieved by rotating anisotropic optical elements [27–31], by electric driving modulation [21, 32], or by division of amplitude [33, 34]. All these methods use totally and uniformly polarized incident light. The polarization state is normally modulated sequentially. In the method proposed here, all possible polarization states are generated at the same time in the beam cross section. We can say that it is a parallel polarization state generator. In the present work we focus on a recently proposed method [35–37] that uses a full Poincaré beam (FPB) [38–40] and the measurement of irradiance across the transverse section of the beam by means of a CCD camera for different configurations of a polarization state analyzer. From these measurements, the Stokes parameters at any point of the input and output beam transverse sections are obtained, and by using their relation, the Mueller matrix of the sample can be determined. Since all possible totally polarized polarization states are present in the cross section of an FPB beam, the invertibility of the polarimetric measurement matrix is guaranteed. We denote this method as Full Poincaré Mueller polarimetry (FPMP) [36, 37]. From the Stokes parameters measured for the input and output beams, there are several alternatives to determine the Mueller matrix of the sample. A first possibility is to take several sets of four pixels in which the polarization states of the input beam coincide with the vertices of a tetrahedron inscribed on the Poincaré sphere and average the results obtained [41]. Another possibility is to consider all pixels in which the irradiance of the input beam exceeds a threshold and use the Moore-Penrose pseudoinverse to determine the Mueller matrix [37]. Here we explore a third possibility based on a Bayesian statistical approach using the Markov chain

Monte Carlo (MCMC) technique.

Bayesian inference for parameter estimation is a powerful tool in which Bayes' theorem is used to update the probability of a hypothesis, including the value of a population parameter, as more evidence or information becomes available [42]. It has been successfully applied in many fields [43] and in particular to polarimetric data reduction [44–52]). In this paper, the Stokes vectors obtained at each pixel of a CCD camera, calculated from the input and output beams images, are used to infer the Mueller matrix elements for several samples. Additionally, several conditions are included for a matrix to represent a physically realizable Mueller matrix [2, 3]. In this work, we propose to combine both full Poincaré Mueller polarimetry with the Mueller matrix recovery using the Bayesian inference approach. The samples that we will use are well known, such as air, phase plates, and polarizers, all homogeneous and transparent, whose theoretical Mueller matrix is known.

The article is structured as follows. In Section 2 we give a brief review of the Full Poincaré Mueller polarimetry technique, as well as different methods (and approximations) used to obtain the Mueller matrix of the sample. In Section 3 we describe the procedure of using Bayesian inference with the obtained data to retrieve the Mueller matrix of the sample. We tested this method with simulated and experimental measurements in Section 4 and finally, in Section 5 we present the most significant conclusions.

2. Full Poincaré Mueller Polarimetry

The polarization of light can be appropriately described by four Stokes parameters, usually arranged in a column vector [2, 53]. When a light beam interacts with a sample, its polarization state changes in a way that depends on the properties of the sample under study. Neglecting nonlinear effects, the polarization change can be described by the Mueller matrix of the sample, which is a 4×4 matrix with real elements. If the polarization state of the input and output beams are denoted by $\mathbf{S}^{\text{out}}$ and $\mathbf{S}^{\text{in}}$, respectively, they are related through the following relation [2, 53]:

$$\mathbf{S}^{\text{out}} = \widehat{M}\,\mathbf{S}^{\text{in}}\,, \tag{1}$$

where $\widehat{M} = \{m_{ij}\}$ $(i, j = 0, 1, 2, 3)$ is the 4×4 Mueller matrix of the sample.

A matrix of 4×4 real values represents a physically realizable Mueller matrix if, for any possible input Stokes vector, it gives a valid output Stokes

vector. Some necessary conditions that a matrix must fulfill to be a physically realizable Mueller matrix are known [2, 3, 53], such as

$$\begin{aligned} \mathrm{Tr}\left(\widehat{M}\widehat{M}^T\right) &\leq 4m_{00}^2, \\ m_{00} &\geq |m_{ij}|, \\ m_{00}^2 &\geq b^2, \\ (m_{00}-b)^2 &\geq \sum_{j=1}^{3}\left(m_{0j}-\sum_{k=1}^{3} m_{jk}a_k\right), \end{aligned} \tag{2}$$

where Tr denotes the trace of a matrix, $b = \sqrt{m_{01}^2 + m_{02}^2 + m_{03}^2}$, and $a_j = m_{0j}/b$. Such constraints will be imposed in the process of recovering the Mueller matrix by Bayesian inference.

For a non-uniformly polarized beam, as is the case for a FPB, Eq. (1) is satisfied for each point across the beam cross section. Then, using an appropriate polarization state analyzer and a CCD camera, all four Stokes parameters of the input and output beams can be measured at the same time across their whole cross section. Since a FPB contains all possible totally polarized states in its cross section, by analyzing the polarization changes in N pixels of the CCD camera, the Mueller matrix of the sample can be recovered [35, 37].

Figure 1 shows the experimental setup for the measurement of the Stokes parameters of the input beam (without any sample) and of the output beam (with a sample inserted). A FPB is generated by focusing a linearly polarized He-Ne laser beam ($\lambda = 632.8$ nm), stabilized both in power and in frequency (Spectra Physics model 117A), onto a calcite crystal with its optical axis along the z direction. The input field is decomposed into ordinary and extraordinary components, whose phase difference at the output crystal face varies with position, giving rise to a non-uniformly polarized beam. The resulting beam has been shown to contain all possible totally polarized polarization states [40]. A detailed description of how this FPB is generated can be found in [40] and [35]. A lens is used to collimate the output beam, which acts as a parallel polarization state generator [35, 40]. The polarization state of the beam (with and without the presence of the sample) is analyzed using a polarizer (P), a quarter-wave plate (QWP), and a CCD camera. A SP620U CCD camera is used to record the experimental images. The pixel size is 4.4 μm, the number of effective pixels is 1600×1200, so that the entire usable area is 7.1×5.4 mm^2. The lowest measurable signal is 2.5 nW/cm^2,

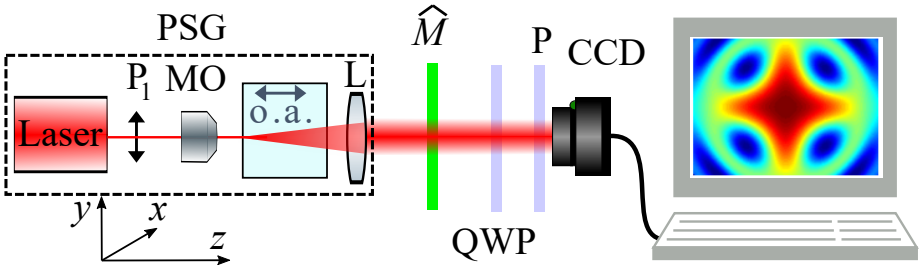

Figure 1: Experimental setup. PSG: polarization state generator; P_1 and P: linear polarizers; MO: microscope objective; L: lens; $\widehat{M}$: sample; QWP: quarter wave plate.

and its dynamic range is over 60 dB. Sets of 10,000 randomly chosen points are sampled in identical pixels for the input and output beams, which are used to estimate the elements of the Mueller matrix of each specimen by applying the technique described in the next section.

The Stokes parameters can be obtained from the measured powers at each pixel of the CCD camera of the experimental setup shown in Fig. 1 as [53]

$$\begin{aligned} S_0 &= \left(P_0 + P_{\pi/2} + P_{\pi/4} + P_{-\pi/4} + P_{\lambda/4,\pi/4} + P_{\lambda/4,-\pi/4}\right)/3, \\ S_1 &= P_0 - P_{\pi/2}, \\ S_2 &= P_{\pi/4} - P_{-\pi/4}, \\ S_3 &= P_{\lambda/4,\pi/4} - P_{\lambda/4,-\pi/4}, \end{aligned} \tag{3}$$

where P_β and $P_{\lambda/4,\beta}$ are the powers measured after a linear polarizer and after a quarter-wave plate (QWP) followed by a linear polarizer, with the subscript β referring to the angle between the x axis and the polarizer transmission axis, while $\lambda/4$ denotes the presence of the QWP with its fast axis at 0 degrees with respect to the x axis [1, 2].

The measured Stokes vectors of the input and output beams can be arranged in two $4 \times N$ matrices, $\widehat{S}^{\text{in}}$ and $\widehat{S}^{\text{out}}$, respectively, which are related by:

$$\widehat{S}^{\text{out}} = \widehat{M}\,\widehat{S}^{\text{in}}, \tag{4}$$

which allows the Mueller matrix to be recovered. Since Stokes parameters are measured across the entire beam cross-section, samples under test are required to be homogeneous, at least in regions not smaller than the beam cross-section.

However, before proceeding with the recovery process, some criteria can be adopted to exclude less significant pixels. The first criterium consists of considering only those pixels where the measured power is above a certain percentage (e.g., 10%) of the maximum [54]. The second one is related to the degree of polarization. The input beam is completely polarized, so that the degree of polarization should be 1 for all pixels. If the samples under study are non-depolarizing, the same argument holds for the output beam. For more general samples, the degree of polarization of the output beam is restricted in any case to the range [0, 1]. However, because of experimental errors, values outside that interval may also be obtained. In this work, we study non-depolarizing elements and we choose to include only those pixels where the measured degree of polarization of the input beam is in the range 1 ± 0.1.

The main sources of error in this polarimetric method are: a possible transverse shift of images, inaccuracy in the intensity measurements, the finite size of the pixels, resulting in an average of the measured values in the area of each pixel [54, 55]. The accuracy of the system is also affected by temporal variations in the intensity distribution across the beam section.

3. Bayesian statistical approach

With the rapid evolution of sensing and measurement methods in polarimetry, obtaining huge amounts of experimental data is becoming commonplace and affordable. The real challenge is to take advantage of this vast information to determine the desired parameters as accurately as possible. Bayesian statistics offers a very convenient mathematical approach to analyzing experimental data and incorporating them into efficient predictive models.

Bayesian inference uses a formulation based on updating the parameter values as the number of available experimental data increases [56]. When handling a large number of data, Bayesian statistics have a higher computational cost than other classical methodologies. However, by using certain algorithms suitable for this type of approach, such as Markov chain Monte Carlo methods [57], a very efficient computational procedure for Bayesian analysis can be achieved, which allows the handling of numerical difficulties initially encountered [58].

In order for the 16 coefficients of the Mueller matrix to be estimated by Bayesian inference, they are all modeled as random variables. This approach

is different from that followed in conventional (frequentist) statistics, where the parameters are not considered as random variables and the uncertainties are represented, for each of them, by confidence intervals.

Our aim is to compute the joint probability density function of the parameters m_{ij} of a matrix $\widehat{M}$, given the available data D and the previous information I: $P\left(\widehat{M} \mid D, I\right)$. Previous information I contains the description of the statistical relations between parameters and data, and also all the prior information available about the parameters, such as the particular relations that make a matrix realizable [see Eq. (2)].

The probability density of the parameters can be constructed using Bayes' theorem [59].

$$P\left(\widehat{M} \mid D, I\right) = \frac{P\left(D \mid \widehat{M}, I\right)}{P(D|I)} P\left(\widehat{M}|I\right) . \tag{5}$$

The term $P\left(\widehat{M}|I\right)$ is named the *prior*, and contains information about the Mueller matrix before obtaining any data. The term $P\left(D \mid \widehat{M}, I\right)$ is the *likelihood*, i.e., the probability of obtaining the data given the parameters. The term $P(D|I)$ is usually called *global likelihood* or *marginal likelihood*. Finally, the probability of the parameters given the data and model, $P\left(\widehat{M} \mid D, I\right)$, is usually called the *posterior*. The Bayesian model is constructed by multiplying the likelihood by the prior and then normalizing it by the global likelihood.

Except in the simplest cases, the global likelihood is very difficult to compute, being the result of marginalization, that is, integrating over the parameters [59]. In our case, this implies an integral in 16 dimensions of the already complicated product of the likelihood and the prior. In general, the difficulty increases geometrically with the number of parameters. Consequently, obtaining the posterior analytically is often unaffordable.

The solution to this problem is to sample from the posterior and use the sampled values as an approximation to the posterior distribution[60]. As we increase the size of the sample, we gradually approach the posterior distribution. In general, for a multidimensional probability distribution, we can calculate any function of its parameters without needing to know the posterior completely [61]. The main difficulty with this procedure is that

we cannot randomly sample from a distribution that is previously unknown. The way to avoid this is to make a dependent sampling, in which the choice of each sampling point depends on the previous point [60].

The way to carry out a dependent sampling is by using the so-called Markov chains [62] to perform a random walk through the parameter space. A Markov chain is a stochastic series of events in which the probability of the occurrence of an event only depends on the immediately preceding event. This dependent sampling is always less efficient than independent sampling, as the informative value of each sampled value is lower than in the independent case [60]. Since the draws within a chain are not independent, the effective sample size will be smaller than the total number of iterations. As the complexity of the model increases, the difference between the effective and actual sample size increases [58]. The important point is that it can be shown [56] that, under certain algorithms to move through the parameter space, the method produces chains of approximate values that converge to the exact target distribution. However, the samples in the Markov chain only represent the target distribution when the chain achieves convergence. Several methods to monitor the convergence of the chains are used in the next section.

Examples of MCMC algorithms are: Metropolis Random Walk, the Metropolis-Hasting algorithm, and Gibbs sampling [56]. There are computing environments for Bayesian inference where the sampling algorithm is already implemented and the user writes the model in a domain specific language. In this work, we use Stan [63, 64] which uses the No-U-Turn sampler (NUTS) [65] as its default sampler. NUTS is an extension of the Hamiltonian Monte Carlo (HMC) algorithm[66, 67].

The HMC algorithm uses geometric information from the posterior to decide how to move through the parameter space, where each point in that space is characterized by the logarithm of the posterior for a set of given parameters. HMC uses Hamiltonian dynamics procedures to mimic the movement of a particle through the potential field computed from the posterior. A random initial momentum allows it to move into regions of high potential and thus traverse the entire parameter space. Since the motion will be strongly influenced by the gradient of the potential, it is necessary to be able to calculate (analytically or numerically) the gradients of the logarithm of the posterior with respect to all parameters. Each point in the chain is subdivided into small discrete steps. It is necessary to make these steps very small or apply a symplectic method so that no divergences appear on the

path of the particles [67]. To computationally implement the equations, the "leapfrog" method [65] has been used. It is a very efficient search algorithm, which will explore the minima of the potential energy, that is, the zones of maximum probability for the posterior, by means of leap proposals that are not symmetric with respect to the initial position but are biased towards the mode of the posterior. This bias will increase as the gradient in the zone increases. The algorithm depends on three parameters: the variances for the initial momentum distribution of each iteration, the number of steps in each iteration, and the time interval at each step. To optimize efficiency, it is necessary to tune these parameters. This is done in a warm-up phase, where you start with certain values and change them to optimize the algorithm. The warm-up phase must be long enough to reach a stable situation. To assess the convergence of the process, several chains are run in parallel. Different values of the above parameters are used in each chain and, once the warm-up phase is finished in each chain, the parameters are not modified during the rest of the calculation.

To summarize, we must provide the statistical model, describing the likelihood and the priors, and Stan performs the sampling parameters tuning during the warm-up phase and the actual sampling.

A flow diagram of the procedure is presented in Fig. 2. It shows how the probability distributions of the posteriors (in this case, the elements of the Mueller matrix) are derived from the input and output Stokes vectors of the considered image pixels. It can be seen that the output Stokes vectors are assumed to arise from a normal distribution around the expected values $\mu_{i,k}$ computed from the input vectors and the Mueller matrix. In this algorithm, $\mu_{i,k}$ are latent variables. The dispersion σ of that normal distribution is another parameter of the model, and it is assumed to be the same for the four elements of the Stokes vectors. The procedure makes use of non-informative priors for the parameters and applies the necessary constraints among the parameter values.

4. Results

To check the applicability to FPMP of the proposed Bayesian method, the latter has been applied to experimental measurements on several known samples. Data input, an initial selection of experimental data, and the handling of output files have been programmed in R [68]. The HMC models have been programmed using the Stan programming language [63, 64].

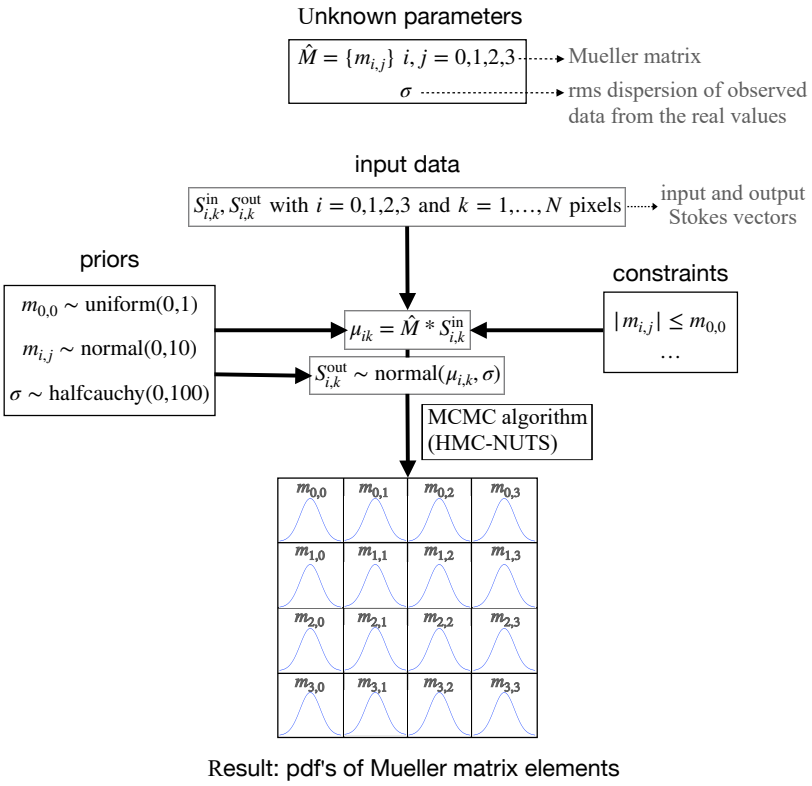

Figure 2: Flowchart of the algorithm.

Stan is a language specially designed for complex statistical models that incorporates, among other components, the NUTS (an extension of HMC) algorithm. As input, we used a random selection of 10,000 pixels from the experimental measurement file. We run in parallel 4 independent Markov chains, each with 1,000 steps for the warm-up phase, followed by 2,000 steps for the parameter sampling. This allows us to check at the end of the calculation whether the chains have converged to the same mean values, within errors, for each parameter obtained. Typical computing time to process sample data on a laptop computer (Mac Apple M1) is about 10 minutes.

Figure 3 (a) represents (for the element m_{00} of the Mueller matrix of a linear polarizer with its transmission axis at 90°, as an example) a trace diagram showing, step by step, the exploration process of the four Markov chains, showing that the chains converge to the same value after a given number of iterations, indicated by a vertical dashed line. From then on,

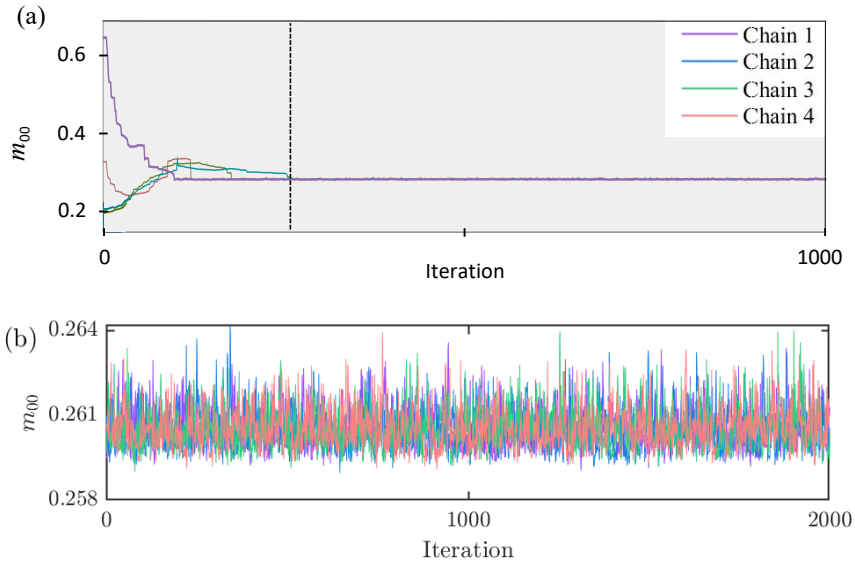

Figure 3: (a) Trace diagram showing the convergence of the 4 Markov chains used by the NUTS algorithm to estimate the element m_{00} of the Mueller matrix of a linear polarizer with its transmission axis at 90°. (b) Trace diagram, for the same element, showing about 2000 steps, after the warm-up phase. The same color code for the chains than in (a) has been used.

the dispersion around the central value of m_{00} provides an estimate of the uncertainty in the measurement of this parameter. The Gelman & Rubin [69] $\hat{\mathrm{R}}$ convergence diagnostic, which compares estimates between and within the chains of model parameters, has been applied (see also [70]). If the chains do not mix well (i.e., the estimates between and within the chains do not agree), $\hat{\mathrm{R}}$ is greater than 1. We have obtained values very close to 1 for all the chains in the 16 parameters calculated. In fact, $\hat{\mathrm{R}}$ ranges from 0.9996 to 1.0010 for this sample. Figure 3 (b) shows the dispersion in the m_{00} values for each step of the calculation after the chains have converged and are completely mixed.

Figure 4 shows the sampled values of the m_{00} parameter against the log-posterior, highlighting in different colors all the 4 Markov chains. The overlapping at the locus of the results for the four chains adds confidence to the method. The same procedure was followed to obtain the 16 elements of the Mueller matrix for each sample analyzed.

The results obtained have been compared to the expected theoretical Mueller matrix in several cases, where air, a quarter-wave phase plate with

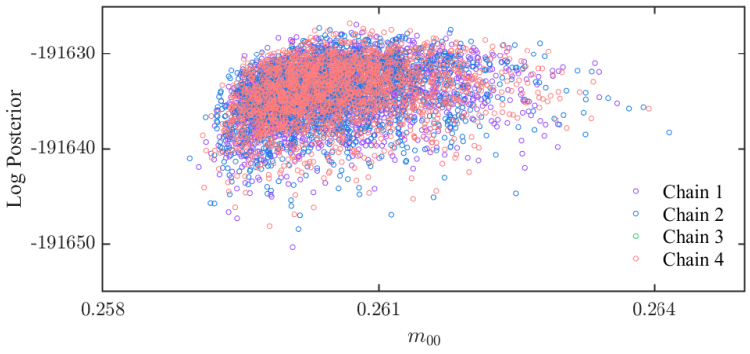

Figure 4: Sampled values of the m_{00} parameter against the log-posterior, highlighting in different colors all the 4 Markov chains, using the NUTS algorithm.

its fast axis at 0°, and a polarizer with its transmission axis at 90° were used as samples. The Mueller matrices of these samples are theoretically known (see [35], for the QWP and the polarizer).

Adding the results of the sampling in the four Markov chains, the applied Bayesian inference method provides the full probability distribution functions (PDF) for the 16 elements of the Mueller matrix, including all the cross-correlations among all the parameters. If the elements of the Mueller matrix are arranged in a row vector $\underline{M} = (m_{00}, m_{01}, \cdots, m_{33})$, their correlation coefficients can be represented in the usual 16×16 correlation matrix (there are 120 different correlations). Fig. 5 shows the results obtained for the linear dichroic polarizer with its transmission axis at 90°. For each pair of coefficients, we show a dispersion diagram with the sampled values, and the diagonal is used to represent the PDF of each Mueller matrix element. It can be seen that only four pairs (from the 120 possible cases) show a certain correlation. Correlated elements are those in the same row in the first and second columns of the Mueller matrix. Due to symmetry considerations on the Mueller matrices, homogeneous noise in the images does not reflect into homogeneous noise that is distributed evenly among the 16 elements of the matrix [71]. This aspect has been noted before [72], and it is expected that some elements of the Mueller matrix are strongly correlated. A similar behavior is observed for all samples.

Note that our technique is not limited to providing a mean value for each parameter or a mean plus a dispersion, but it provides a full PDF. In this sense, although most of the histograms on the diagonal of Fig. 5 seem sym-

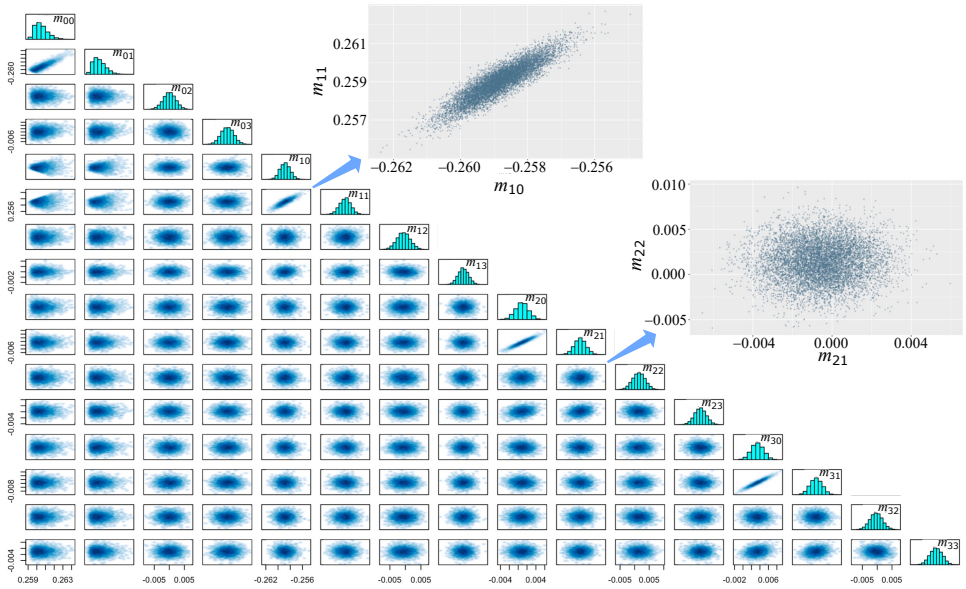

Figure 5: Cross-correlations of the elements of the Mueller matrix for a polarizer with its transmission axis at 90°. The two magnified plots in the upper half of the panel correspond to examples of high and low correlation between elements.

metric, some elements exhibit a more complex distribution that cannot be summarized by just two numbers (such as the mean and the standard deviation). For this reason, it is always better to report the derived PDF, which comprises a full characterization of the parameters. In any case, if we want to summarize the results of the analysis using a limited set of descriptive measurements to characterize a general probability distribution, we recommend using the median as a centralization measurement (more robust than the arithmetic mean), the MAD (mean absolute deviation) as a measurement of the dispersion instead of the rms standard deviation, and the Highest Density Interval (HDI) as an alternative to the conventional confidence interval to cope with nonsymmetrical distributions. The HDI is the Bayesian counterpart of the classical confidence interval. It is a credible interval defined as the narrowest interval that includes a given percentage (e.g., 95%) of the posterior probability distribution of the parameter. It represents the range of values with the highest probability density, providing a robust and informative measure of uncertainty. See, for example, [73] for a definition and discussion of HDI.

The results of the analysis of the experimental data for three samples are shown in Figs. 6, 7, and 8. In these three figures, green dashed vertical lines represent the median values for the PDFs of the elements in the Mueller matrix of each sample, while black dashed vertical lines indicate the expected values for these samples [37]. The 95% HDI for each element is denoted as a solid horizontal red bar.

Figure 6 shows the results for a linear polarizer with its transmission axis at 90°. The horizontal scale interval in all histograms is set at 0.016, so it can be seen that the PDF of some elements is narrower than for the rest. In particular, the PDF's are very narrow for the four elements whose theoretical value is ±0.26. In fact, the HDI width of these four elements is very small (less than 0.003). Moreover, the absolute value of the difference between the median and the theoretical value is less than 0.004 for all elements. Note also that the theoretical values are within or very close to the calculated HDI for the sixteen elements of the Mueller matrix.

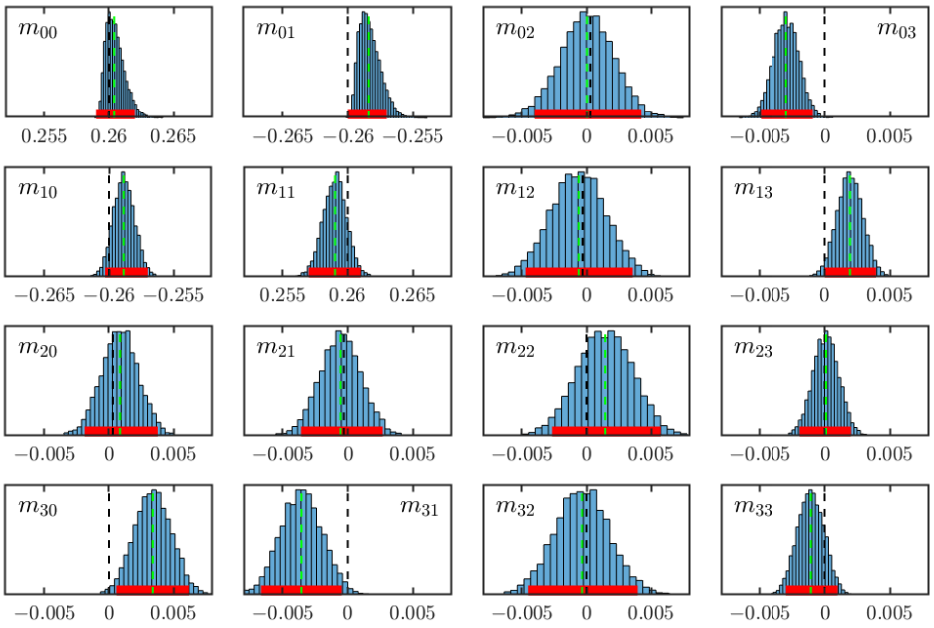

Figure 6: Histograms for the elements of the Mueller matrix for a linear dichroic polarizer with its transmission axis at 90°. The dashed green line denotes the median, the red bar represents the 95% HDI and the dashed black line represents the theoretical expected value for each element.

For the case of air, Fig. 7 shows the histograms of the elements of the Mueller matrix obtained from the analysis of the experimental measurements of this sample. In this case, the value of $\hat{\mathrm{R}}$ for the 16 elements of the Mueller matrix is in the interval [0.9996, 1.0012]. For a better visualization of these histograms, different intervals of the horizontal scale have been used. In particular, for elements m_{00} and m_{33} the interval is 0.003, and 0.011 for the rest. In any case, the histograms for this sample are, in general, narrower than for the polarizer. The experimental values obtained for the elements of the Mueller matrix are quite close to the expected ones, especially for the null elements (for these elements the maximum difference is 0.002) and slightly higher for the two of the non-null elements (the elements of the main diagonal should be one). It should be noted that the histogram of the elements m_{00} and m_{33} is rather asymmetric, which may be an effect of the restrictions imposed on the physical realizability of the Mueller matrices [see Eq. (2)].

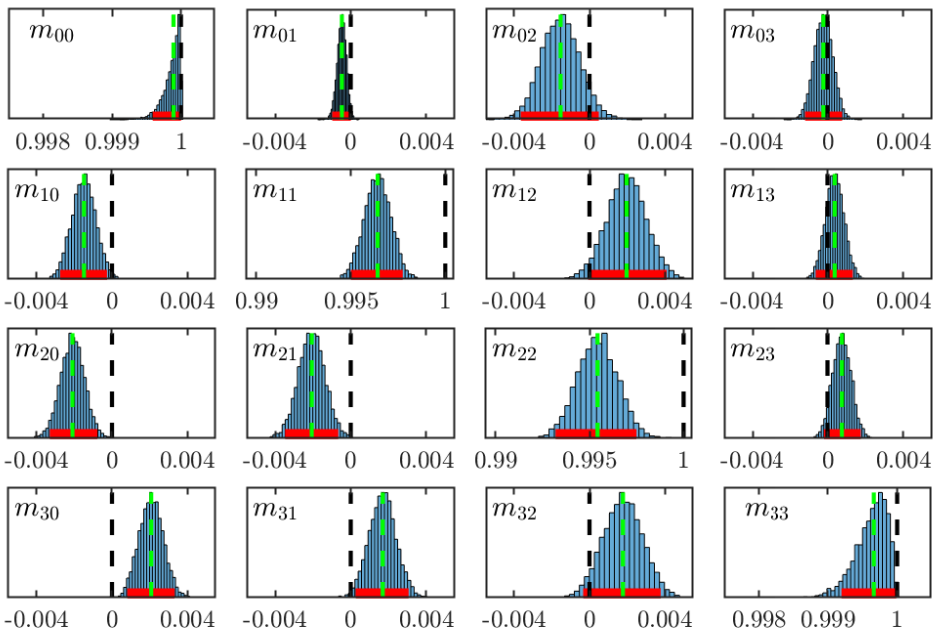

Figure 7: Histograms for the elements of the Mueller matrix for the air. The dashed green line denotes the median, the red bar represents the 95% HDI and the dashed black line represents the theoretical expected value for each element.

Finally, Fig. 8 shows the results obtained for the quarter-phase wave plate

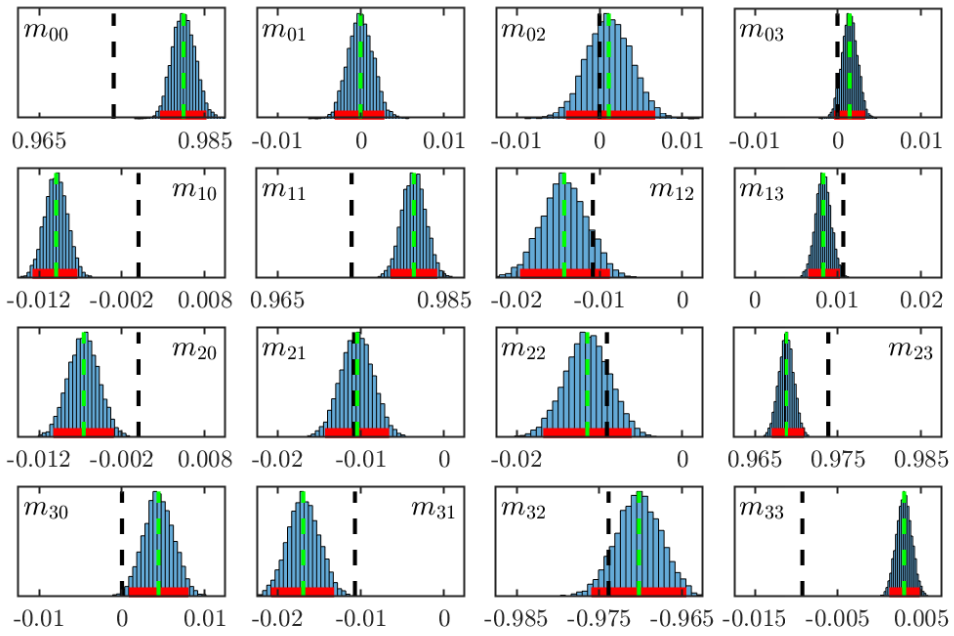

Figure 8: Histograms for the elements of the Mueller matrix for a quarter phase plate with its axis at 0°. The dashed green line denotes the median, the red bar represents the 95% HDI and the dashed black line represents the theoretical expected value for each element.

with its fast axis at 0° (see Fig. 8). For this sample, the value of $\hat{\mathrm{R}}$ ranges from 0.9997 to 1.0011. In this case, the horizontal scale interval is 0.025 for all elements and this scale has been shifted so that the expected theoretical value is close to the center of the graph. For this sample, the maximum HDI width is 0.011 and the differences between experimental and theoretical values are lower than 0.012. These differences, which are greater in this sample than in the others, could be due to different sources of error, such as some misalignment of the fast axis of the sample and a possible transverse displacement of the images taken by the CCD camera, which may occur if the input beam is not perfectly perpendicular to the sample [55].

Similar Mueller matrices have been obtained for these samples using the Moore-Penrose pseudoinverse [37]. However, in the Bayesian approach, the PDF of each of the sought parameters is constructed from the experimental measurements and from the modeling of the particular problem. In our case, the model is determined by the relation of Eq. (1) and must also satisfy the

realizability conditions given in Eq (2). In summary, the Bayesian inference approach provides, for each observational dataset, a large set of Mueller matrices (as many as the number of steps in the chains), which allows us to perform a robust estimation of their associated uncertainties and a study of the possible correlations among parameters.

Mueller matrix polarimetry based on polarization modulation with rotating elements has yielded values that differ by less than 0.002 [30, 31] from the theoretical values for air. Similar accuracy has also been achieved with the use of polarimeters of amplitude division [25]. Other authors report differences of less than 0.014 [21] or 0.5% [74] for electrically driven modulation polarimeters.

5. Conclusions

A Bayesian approach has been proposed to analyze a large amount of experimental full Poincaré Mueller polarimetry data. Using a polarization analyzer and a CCD camera, maps of the Stokes parameters in the beam cross section at the entrance and exit of a sample are obtained. These data have been processed by Bayesian inference to determine the 16 elements of the Mueller matrix of the sample. One of the advantages of Bayesian analysis is its flexibility in specifying suitable models for the data. This flexibility allows us to impose several necessary conditions that a matrix must satisfy to represent a physically realizable Mueller matrix.

It should be noted that Bayesian analysis has the ability to generate computationally robust estimates of the parameter values and their credible intervals. As a result, the procedure provides the full probability density function for each element of the Mueller matrix. If necessary, this PDF can be summarized by reporting a central value along with an interval of the highest probability density (HDI). Also, the procedure provides the correlation values between all pairs of elements. The credible intervals do not depend on the large-N approximations, nor do the credible intervals depend on the intended tests.

Finally, applying this method to three different test samples (air, a quarter-wave phase plate with its fast axis at 0° and a polarizer with its transmission axis at 90°) yields values of their Mueller matrices very close to the expected theoretical ones. Moreover, very narrow credible intervals are found for all elements. Therefore, Bayesian inference is a very useful tool for determining

the Mueller matrix when a large number of independent experimental data are measured, as is the case for full Poincaré polarimetry.

Acknowledgements

This work has been supported by Spanish Ministerio de Economía y Competitividad under projects PID2019-104268GB-C21, PID2019-107427GB-C31 and PID2021-123417OB-I00.

References

[1] R. M. A. Azzam, Stokes-vector and Mueller-matrix polarimetry [Invited], J. Opt. Soc. Am. A 33 (7) (2016) 1396–1408. doi:10.1364/JOSAA.33.001396.
URL http://josaa.osa.org/abstract.cfm?URI=josaa-33-7-1396

[2] R. Chipman, W. Lam, G. Young, Polarized Light and Optical Systems, Optical Sciences and Applications of Light, CRC Press, 2018.
URL https://books.google.es/books?id=KwFlDwAAQBAJ

[3] J. J. Gil, R. Ossikovski, Polarized Light and the Mueller Matrix Approach, CRC Press Taylor & Francis Group, Boca Raton, 2016. doi:10.1201/b19711.

[4] C. He, H. He, J. Chang, B. Chen, H. Ma, M. J. Booth, Polarisation optics for biomedical and clinical applications: a review, Light: Science & Applications 10 (09 2021). doi:10.1038/s41377-021-00639-x.
URL https://doi.org/10.1038/s41377-021-00639-x

[5] J. C. G. de Sande, A. Rodríguez, T. Rodríguez, Spectroscopic ellipsometry determination of the refractive index of strained $Si_{1-x}Ge_x$ layers in the near-infrared wavelength range (0.9—1.7μm), Applied Physics Letters 67 (23) (1995) 3402–3404. doi:http://dx.doi.org/10.1063/1.114907.
URL http://scitation.aip.org/content/aip/journal/apl/67/23/10.1063/1.114907

[6] J. C. G. de Sande, R. Serna, J. Gonzalo, C. N. Afonso, D. E. Hole, A. Naudon, Refractive index of Ag nanocrystals composite films in the neighborhood of the surface plasmon resonance, Journal of Applied

Physics 91 (3) (2002) 1536–1541. arXiv:https://doi.org/10.1063/1.1427404, doi:10.1063/1.1427404.
URL https://doi.org/10.1063/1.1427404

[7] G. López-Morales, M. d. M. Sánchez-López, A. Lizana, I. Moreno, J. Campos, Mueller matrix polarimetric imaging analysis of optical components for the generation of cylindrical vector beams, Crystals 10 (12) (2020). doi:10.3390/cryst10121155.
URL https://www.mdpi.com/2073-4352/10/12/1155

[8] S. K. Ray, N. Ghosh, A. Vitkin, Diattenuation and retardance signature of plasmonic gold nanorods in turbid media revealed by Mueller matrix polarimetry, Scientific Reports 11 (1) (2021) 20017. doi:10.1038/s41598-021-99430-6.
URL https://doi.org/10.1038/s41598-021-99430-6

[9] V. Tiwari, N. S. Bisht, Combined Jones-Stokes polarimetry and its decomposition into associated anisotropic characteristics of spatial light modulator, PHOTONICS 9 (3) (MAR 2022). doi:10.3390/photonics9030195.

[10] V. V. Tuchin, L. Wang, D. A. Zymnayakov, Optical Polarization in Biomedical Applications, Springer, 2006.

[11] N. Ghosh, A. I. Vitkin, Tissue polarimetry: concepts, challenges, applications, and outlook, Journal of Biomedical Optics 16 (11) (2011) 1 – 30. doi:10.1117/1.3652896.
URL https://doi.org/10.1117/1.3652896

[12] S. Alali, A. Gribble, I. A. Vitkin, Rapid wide-field Mueller matrix polarimetry imaging based on four photoelastic modulators with no moving parts, Opt. Lett. 41 (5) (2016) 1038–1041. doi:10.1364/OL.41.001038.
URL http://opg.optica.org/ol/abstract.cfm?URI=ol-41-5-1038

[13] W. Sheng, W. Li, J. Qi, T. Liu, H. He, Y. Dong, S. Liu, J. Wu, D. S. Elson, H. Ma, Quantitative analysis of 4×4 Mueller matrix transformation parameters for biomedical imaging, PHOTONICS 6 (1) (MAR 26 2019). doi:10.3390/photonics6010034.

[14] V. N. D. Le, I. Saytashev, S. Saha, P. F. Lopez, M. Laughrey, J. C. Ramella-Roman, Depth-resolved Mueller matrix polarimetry

microscopy of the rat cornea, Biomed. Opt. Express 11 (10) (2020) 5982–5994. doi:10.1364/BOE.402201.
URL http://opg.optica.org/boe/abstract.cfm?URI=boe-11-10-5982

[15] R. N. Huynh, G. Nehmetallah, C. B. Raub, Mueller matrix polarimetry and polar decomposition of articular cartilage imaged in reflectance, Biomed. Opt. Express 12 (8) (2021) 5160–5178. doi:10.1364/BOE.428223.
URL http://opg.optica.org/boe/abstract.cfm?URI=boe-12-8-5160

[16] H. Kobayashi, M. Hayashi, K. Shiraishi, Y. Nakura, T. Enomoto, K. Miura, H. Takahashi, Y. Igarashi, H. Naoe, N. Kaneyasu, T. Nishizawa, N. Sugimoto, Development of a polarization optical particle counter capable of aerosol type classification, Atmospheric Environment 97 (2014) 486–492. doi:https://doi.org/10.1016/j.atmosenv.2014.05.006.
URL https://www.sciencedirect.com/science/article/pii/S1352231014003537

[17] D. Li, F. Chen, N. Zeng, Z. Qiu, H. He, Y. He, H. Ma, Study on polarization scattering applied in aerosol recognition in the air, Opt. Express 27 (12) (2019) A581–A595. doi:10.1364/OE.27.00A581.
URL http://opg.optica.org/oe/abstract.cfm?URI=oe-27-12-A581

[18] S. Qi, Z. Huang, X. Ma, J. Huang, T. Zhou, S. Zhang, Q. Dong, J. Bi, J. Shi, Classification of atmospheric aerosols and clouds by use of dual-polarization lidar measurements, Opt. Express 29 (15) (2021) 23461–23476. doi:10.1364/OE.430456.
URL http://opg.optica.org/oe/abstract.cfm?URI=oe-29-15-23461

[19] I. Sierra, M. R. Chialanza, R. Faccio, D. Carrizo, L. Fornaro, A. Pérez-Parada, Identification of microplastics in wastewater samples by means of polarized light optical microscopy, Environmental Science and Pollution Research 27 (7) (2020) 7409–7419. doi:10.1007/s11356-019-07011-y.
URL https://doi.org/10.1007/s11356-019-07011-y

[20] J. S. Baba, J.-R. Chung, A. H. DeLaughter, B. D. Cameron, G. L. Cote, Development and calibration of an automated Mueller matrix polarization imaging system, Journal of Biomedical Optics 7 (2002) 7 – 7 – 9. doi:10.1117/1.1486248.
URL http://dx.doi.org/10.1117/1.1486248

[21] J. M. Bueno, Polarimetry using liquid-crystal variable retarders: theory and calibration, Journal of Optics A: Pure and Applied Optics 2 (3) (2000) 216.
URL http://stacks.iop.org/1464-4258/2/i=3/a=308

[22] O. Arteaga, R. Ossikovski, E. Kuntman, M. A. Kuntman, A. Canillas, E. Garcia-Caurel, Mueller matrix polarimetry on a Young's double-slit experiment analog, Opt. Lett. 42 (19) (2017) 3900–3903. doi:10.1364/OL.42.003900.
URL http://ol.osa.org/abstract.cfm?URI=ol-42-19-3900

[23] J. C. G. de Sande, M. Santarsiero, G. Piquero, Spirally polarized beams for polarimetry measurements of deterministic and homogeneous samples, Optics and Lasers in Engineering 91 (2017) 97 – 105. doi:http://dx.doi.org/10.1016/j.optlaseng.2016.11.008.
URL http://www.sciencedirect.com/science/article/pii/S0143816616304171

[24] J. C. G. de Sande, G. Piquero, M. Santarsiero, Polarimetry with azimuthally polarized light, Optics Communications 410 (2018) 961 – 965. doi:https://doi.org/10.1016/j.optcom.2017.10.002.
URL http://www.sciencedirect.com/science/article/pii/S003040181730888X

[25] J. del Hoyo, L. M. Sanchez-Brea, J. A. Gomez-Pedrero, High precision calibration method for a four-axis Mueller matrix polarimeter, Optics and Lasers in Engineering 132 (2020) 106112. doi:https://doi.org/10.1016/j.optlaseng.2020.106112.
URL https://www.sciencedirect.com/science/article/pii/S0143816619318263

[26] E. Nabadda, G. López-Morales, D. Marco, M. del Mar Sánchez-López, I. Moreno, Mueller matrix polarimetric analysis applied

to characterize the physical parameters of a twisted-nematic liquid–crystal modulator, Optics & Laser Technology 156 (2022) 108567. doi:https://doi.org/10.1016/j.optlastec.2022.108567.
URL https://www.sciencedirect.com/science/article/pii/S0030399222007162

[27] R. Azzam, A simple Fourier photopolarimeter with rotating polarizer and analyzer for measuring Jones and Mueller matrices, Optics Communications 25 (2) (1978) 137–140. doi:https://doi.org/10.1016/0030-4018(78)90291-2.
URL https://www.sciencedirect.com/science/article/pii/0030401878902912

[28] K. M. Twietmeyer, R. A. Chipman, Optimization of Mueller matrix polarimeters in the presence of error sources, Opt. Express 16 (15) (2008) 11589–11603. doi:10.1364/OE.16.011589.
URL http://www.opticsexpress.org/abstract.cfm?URI=oe-16-15-11589

[29] S. G. Reddy, S. Prabhakar, A. Aadhi, A. Kumar, M. Shah, R. P. Singh, R. Simon, Measuring the Mueller matrix of an arbitrary optical element with a universal SU(2) polarization gadget, J. Opt. Soc. Am. A 31 (3) (2014) 610–615. doi:10.1364/JOSAA.31.000610.
URL http://josaa.osa.org/abstract.cfm?URI=josaa-31-3-610

[30] H. Gu, X. Chen, H. Jiang, C. Zhang, S. Liu, Optimal broadband Mueller matrix ellipsometer using multi-waveplates with flexibly oriented axes, Journal of Optics 18 (2) (2016) 025702. doi:10.1088/2040-8978/18/2/025702.
URL https://dx.doi.org/10.1088/2040-8978/18/2/025702

[31] H. Gu, H. Jiang, X. Chen, C. Zhang, S. Liu, Superachromatic polarization modulator for stable and complete polarization measurement over an ultra-wide spectral range, Opt. Express 30 (9) (2022) 15113–15133. doi:10.1364/OE.456290.
URL https://opg.optica.org/oe/abstract.cfm?URI=oe-30-9-15113

[32] A. D. Martino, Y.-K. Kim, E. Garcia-Caurel, B. Laude, B. Drévillon, Optimized Mueller polarimeter with liquid crystals, Opt. Lett. 28 (8)

(2003) 616–618. doi:10.1364/OL.28.000616.
URL http://ol.osa.org/abstract.cfm?URI=ol-28-8-616

[33] R. Azzam, Division-of-amplitude photopolarimeter (doap) for the simultaneous measurement of all four Stokes parameters of light, Optica Acta: International Journal of Optics 29 (5) (1982) 685–689. arXiv:https://doi.org/10.1080/713820903, doi:10.1080/713820903.
URL https://doi.org/10.1080/713820903

[34] E. Compain, S. Poirier, B. Drevillon, General and self-consistent method for the calibration of polarization modulators, polarimeters, and Mueller-matrix ellipsometers, Appl. Opt. 38 (16) (1999) 3490–3502. doi:10.1364/AO.38.003490.
URL http://ao.osa.org/abstract.cfm?URI=ao-38-16-3490

[35] J. C. Suárez-Bermejo, J. C. G. de Sande, M. Santarsiero, G. Piquero, Mueller matrix polarimetry using full Poincaré beams, Optics and Lasers in Engineering 122 (2019) 134 – 141. doi:https://doi.org/10.1016/j.optlaseng.2019.05.030.
URL http://www.sciencedirect.com/science/article/pii/S0143816619302805

[36] J. C. G. de Sande, G. Piquero, J. C. Suárez-Bermejo, M. Santarsiero, Mueller matrix polarimetry with invariant polarization pattern beams, Photonics 8 (11) (2021). doi:10.3390/photonics8110491.
URL https://www.mdpi.com/2304-6732/8/11/491

[37] J. C. Suárez-Bermejo, J. C. González de Sande, G. Piquero, A. V. Failla, M. Santarsiero, Full Poincaré Mueller polarimetry using a CCD camera, Photonics 9 (10) (2022) 702. doi:10.3390/photonics9100702.
URL http://dx.doi.org/10.3390/photonics9100702

[38] A. M. Beckley, T. G. Brown, M. A. Alonso, Full Poincaré beams II: partial polarization, Opt. Express 20 (9) (2012) 9357–9362. doi:10.1364/OE.20.009357.
URL http://www.opticsexpress.org/abstract.cfm?URI=oe-20-9-9357

[39] E. J. Galvez, S. Khadka, W. H. Schubert, S. Nomoto, Poincaré-beam patterns produced by nonseparable superpositions of Laguerre-Gauss

and polarization modes of light, Appl. Opt. 51 (15) (2012) 2925–2934. doi:10.1364/AO.51.002925.
URL http://ao.osa.org/abstract.cfm?URI=ao-51-15-2925

[40] G. Piquero, L. Monroy, M. Santarsiero, M. Alonzo, J. C. G. de Sande, Synthesis of full Poincaré beams by means of uniaxial crystals, Journal of Optics 20 (6) (2018) 065602.
URL http://stacks.iop.org/2040-8986/20/i=6/a=065602

[41] Suárez-Bermejo, Juan Carlos, González de Sande, J. Carlos, Santarsiero, Massimo, Piquero, Gemma, Experimental Mueller matrix polarimetry with full Poincaré beams and a CCD camera, EPJ Web Conf. 255 (2021) 12005. doi:10.1051/epjconf/202125512005.
URL https://doi.org/10.1051/epjconf/202125512005

[42] S. E. Fienberg, When did Bayesian inference become "Bayesian"?, Bayesian Analysis 1 (1) (2006). doi:10.1214/06-ba101.

[43] R. v. d. Schoot, S. Depaoli, R. King, B. Kramer, K. Märtens, M. G. Tadesse, M. Vannucci, A. Gelman, D. Veen, J. Willemsen, C. Yau, Bayesian statistics and modelling, Nature Reviews Methods Primers 1 (1) (2021) 1. doi:10.1038/s43586-020-00001-2.

[44] C. Collet, J. Zallat, Y. Takakura, Clustering of Mueller matrix images for skeletonized structure detection, Opt. Express 12 (7) (2004) 1271–1280. doi:10.1364/OPEX.12.001271.
URL https://opg.optica.org/oe/abstract.cfm?URI=oe-12-7-1271

[45] J. Zallat, C. Heinrich, M. Petremand, A Bayesian approach for polarimetric data reduction: the Mueller imaging case, Opt. Express 16 (10) (2008) 7119–7133. doi:10.1364/OE.16.007119.
URL https://opg.optica.org/oe/abstract.cfm?URI=oe-16-10-7119

[46] G. Sfikas, C. Heinrich, J. Zallat, C. Nikou, N. Galatsanos, Recovery of polarimetric Stokes images by spatial mixture models, J. Opt. Soc. Am. A 28 (3) (2011) 465–474. doi:10.1364/JOSAA.28.000465.
URL https://opg.optica.org/josaa/abstract.cfm?URI=josaa-28-3-465

[47] J. L. Quinn, Bayesian analysis of polarization measurements, Astronomy & Astrophysics 538 (2011) A65. doi:10.1051/0004-6361/201015785.
URL https://opg.optica.org/josaa/abstract.cfm?URI=josaa-28-3-465

[48] R. D. Ramkhalawon, T. G. Brown, M. A. Alonso, Imaging the polarization of a light field, Opt. Express 21 (4) (2013) 4106–4115. doi:10.1364/OE.21.004106.
URL https://opg.optica.org/oe/abstract.cfm?URI=oe-21-4-4106

[49] E. Lopez-Rodriguez, Dichroic polarization at mid-infrared wavelengths: a Bayesian approach, Monthly Notices of the Royal Astronomical Society 455 (3) (2015) 2656–2661. arXiv:https://academic.oup.com/mnras/article-pdf/455/3/2656/9386413/stv2747.pdf, doi:10.1093/mnras/stv2747.
URL https://doi.org/10.1093/mnras/stv2747

[50] S. Song, B. Xu, J. Yang, Ship detection in polarimetric SAR images via variational Bayesian inference, IEEE Journal of Selected Topics in Applied Earth Observations and Remote Sensing 10 (6) (2017) 2819–2829. doi:10.1109/JSTARS.2017.2687473.

[51] M. Hohmann, A. Karabayir, P. Herzler, M. Späth, F. Klämpfl, M. Schmidt, Analysis of diffuse reflectance spectroscopy by means of Bayesian inference and separation of the parameters for scattering strength and spectral dependence of the scattering, Journal of Biophotonics 14 (12) (2021) e202100205. arXiv:https://onlinelibrary.wiley.com/doi/pdf/10.1002/jbio.202100205, doi:https://doi.org/10.1002/jbio.202100205.
URL https://onlinelibrary.wiley.com/doi/abs/10.1002/jbio.202100205

[52] L. Smalakys, A. Melninkaitis, Predicting lifetime of optical components with Bayesian inference, Opt. Express 29 (2) (2021) 903–915. doi:10.1364/OE.410844.
URL https://opg.optica.org/oe/abstract.cfm?URI=oe-29-2-903

[53] D. H. Goldstein, Polarized Light, second (revised and expanded) Edition, Marcel Dekker, Inc., 2003.

[54] J. C. Suárez-Bermejo, J. C. G. de Sande, M. Santarsiero, G. Piquero, Effects of Intensity Inaccuracy Measurements in Mueller Matrix Polarimetry with Full Poincaré Beams and a CCD Camera, IFSA Publishing, S.L., 2021, Ch. 3, pp. 163–178.
URL https://www.sensorsportal.com/HTML/BOOKSTORE/Advances_in_Optics_Vol_5.pdf

[55] J. C. Suárez-Bermejo, J. C. G. de Sande, M. Santarsiero, G. Piquero, Analysis of the errors in polarimetry with full Poincaré beams, in: 2019 PhotonIcs Electromagnetics Research Symposium - Spring (PIERS-Spring), 2019, pp. 2621–2627.

[56] A. Gelman, J. B. Carlin, H. S. Stern, D. B. Dunson, A. Vehtari, D. B. Rubin, Bayesian Data Analysis, Chapman & Hall, 2013.

[57] W. Gilks, S. Richardson, D. J. Spiegelhalter, Markov Chain Monte Carlo in Practice, Chapman and Hall : CRC Press, 1996.

[58] C. J. Geyer, Introduction to Markov chain Monte Carlo, Handbook of Markov Chain Monte Carlo, CRC Press, 2011.

[59] D. V. Lindley, Understanding Uncertainty, Wiley, 2013.

[60] M. Y. Wang, T. Park, A Brief Tour of Bayesian Sampling Methods, Bayesian Inference on Complicated Data, 2020.

[61] K. J. Tierney L, Accurate approximations for posterior moments and marginal densities, Journal of the American Statistical Association 81 (393) (1986).

[62] S. Brooks, A. Gelman, G. Jones, X.-L. Meng (Eds.), Handbook of Markov Chain Monte Carlo, Routledge, 2011.

[63] Stan Development Team. Stan modeling language users guide and reference manual [online] (2022).

[64] Stan Development Team, RStan: the R interface to Stan, R package version 2.21.8 (2023).
URL https://mc-stan.org/

[65] A. G. M.D. Hoffman, The No-U-Turn Sampler: Adaptively setting path lengths in Hamiltonian Monte Carlo, Journal of Machine Learning Research 15 (2014) 1593–1623.

[66] S. Duane, A. Kennedy, B. J. Pendleton, D. Roweth, Hybrid Monte Carlo, Physics Letters B 195 (2) (1987) 216–222. doi:https://doi.org/10.1016/0370-2693(87)91197-X.
URL https://www.sciencedirect.com/science/article/pii/037026938791197X

[67] R. M. Neal, MCMC Using Hamiltonian Dynamics, Handbook of Markov Chain Monte Carlo, Rourledge, 2011.

[68] R Core Team, R: A Language and Environment for Statistical Computing, R Foundation for Statistical Computing, Vienna, Austria (2021).
URL https://www.R-project.org/

[69] A. Gelman, D. B. Rubin, Inference from iterative simulation using multiple sequences (with discussion), Statistical Science 7 (4) (1992) 457–511,.

[70] A. Vehtari, A. Gelman, D. Simpson, B. Carpenter, P.-C. Bürkner, Rank-Normalization, Folding, and Localization: An Improved $\widehat{R}$ for Assessing Convergence of MCMC (with Discussion), Bayesian Analysis 16 (2) (2021) 667 – 718. doi:10.1214/20-BA1221.
URL https://doi.org/10.1214/20-BA1221

[71] Y. Takakura, J. E. Ahmad, Noise distribution of Mueller matrices retrieved with active rotating polarimeters, Appl. Opt. 46 (30) (2007) 7354–7364. doi:10.1364/AO.46.007354.
URL https://opg.optica.org/ao/abstract.cfm?URI=ao-46-30-7354

[72] S. N. Savenkov, K. E. Yushtin, Mueller matrix elements error distribution for polarimetric measurements, in: J. A. Shaw, J. S. Tyo (Eds.), Polarization Science and Remote Sensing, Vol. 5158, International Society for Optics and Photonics, SPIE, 2003, pp. 251 – 259. doi:10.1117/12.505632.
URL https://doi.org/10.1117/12.505632

[73] J. Kruschke, Doing Bayesian Data Analysis (Second Edition), Academic Press, Boston, 2015.

[74] O. Arteaga, J. Freudenthal, B. Wang, B. Kahr, Mueller matrix polarimetry with four photoelastic modulators: theory and calibration, Appl. Opt. 51 (28) (2012) 6805–6817. doi:10.1364/AO.51.006805.
URL https://opg.optica.org/ao/abstract.cfm?URI=ao-51-28-6805